Electronic band structure of isolated and bundled carbon nanotubes

S. Reich and C. Thomsen
Institut für Festkörperphysik, Technische Universität Berlin, Hardenbergstr. 36, 10623 Berlin, Germany

P. Ordejón
Institut de Ciència de Materials de Barcelona (CSIC), Campus de la U.A.B. E-08193 Bellaterra, Barcelona, Spain

(Received 25 September 2001; published 29 March 2002)

We study the electronic dispersion in chiral and achiral isolated nanotubes as well as in carbon nanotube bundles. The curvature of the nanotube wall is found not only to reduce the band gap of the tubes by hybridization, but also to alter the energies of the electronic states responsible for transitions in the visible energy range. Even for nanotubes with larger diameters (1–1.5 nm) a shift of the energy levels of ≈ 100 meV is obtained in our *ab initio* calculations. Bundling of the tubes to ropes results in a further decrease of the energy gap in semiconducting nanotubes; the bundle of (10,0) nanotubes is even found to be metallic. The intratube dispersion, which is on the order of 100 meV, is expected to significantly broaden the density of states and the optical absorption bands in bundled tubes. We compare our results to scanning tunneling microscopy and Raman experiments, and discuss the limits of the tight-binding model including only π orbitals of graphene.

DOI: 10.1103/PhysRevB.65.155411 PACS number(s): 71.20.Tx, 73.21.−b, 71.15.Mb

I. INTRODUCTION

The electronic structure of carbon nanotubes is characterized by a series of bands arising from the confinement around the nanotube's circumference. The critical points in isolated nanotubes, which are at the Γ point, the Brillouin-zone boundary, and sometimes also at $k_z \approx 2\pi/3$, give rise to the square-root-like singularities in the density of states typical for one-dimensional systems.[1,2] These singularities were directly studied by scanning tunneling experiments.[3–5] Recently more subtle structures like the secondary gap at the Fermi level were also observed.[6] Ouyang *et al.*[6] compared the density of states of an (8,8) nanotube isolated on a substrate with one residing on top of a tube bundle. They showed that, indeed, a secondary gap opens up in bundled armchair tubes as predicted by Delaney *et al.*[7,8] The second experimental method used widely to study the electronic dispersion encompasses optical experiments and Raman scattering.[9–13] Naturally, optical methods probe the electronic dispersion only indirectly via absorption from the valence to conduction states. When the experimental findings are compared to a theoretical band structure, usually a tight-binding approximation of the graphite π orbitals is employed.[1,14–16] The electronic energies obtained in this approximation are the same as those of the π states of graphite with that tight-binding model, when the boundary conditions around the circumference are considered. This simple picture is frequently expanded to small tubes (diameter $d \lesssim 10$ Å) and to bundles of tubes, although Blase *et al.*[17] showed convincingly that rehybridization has a significant effect on the electronic states. Also ignored in this approach are intramolecular dispersions which are known to be quite large in solid C_{60} and graphite.[18,19] On the other hand, first-principles studies, which do not have these deficiencies, of the electronic bands in ideal carbon nanotubes are extremely rare. Blase *et al.*[17] studied the rehybridization effects in small zigzag nanotubes. They showed that the curvature of the nanotube wall strongly alters the band structure by mixing the π^* and σ^* graphene states. In contrast, Mintmire and White concluded from all-electron calculations of armchair tubes that the differences between first principles and tight-binding calculations are negligible for small enough energies.[20] The tight-binding overlap integral $\gamma_0 = 2.5$ eV, which they extracted from their calculations, agrees nicely with scanning tunneling microscopy (STM) measurements, but is 15% smaller than the value found in optical experiments.[9,10] Combined density-functional-theory (DFT) and parametrized techniques were used to calculate the electronic band structure of bundles of (10,10) tubes.[8,21] These studies focused on valence- and conduction-band crossing at the Fermi level and the secondary gap in bundled armchair tubes.

Here we report on a detailed study of the band structure of single walled nanotubes and nanotube bundles. We calculated the electronic dispersion for achiral as well as chiral nanotubes to investigate the effects of curvature and intertube interaction on the electronic properties. The curvature-induced σ-π hybridization is found to have the most pronounced effects on zigzag nanotubes, where we find a strong downshift of the conduction bands, whereas the electronic band structure is less affected in armchair and chiral nanotubes. Bundling of the nanotubes to ropes further decreases the separation of the conduction and valence bands around the Fermi level. The dispersion perpendicular to the nanotube axis is of similar strength as in other π-bonded carbon material ranging from 200 meV, as calculated for bundles of chiral tubes to 1 eV in armchair nanotube bundles. We compare our findings to scanning tunneling and optical experiments. In particular, we discuss the limits of the tight-binding approximation, neglecting the curvature of the nanotube wall and the coupling between the tubes in a nanorope.

In Sec. II we describe the computational method used in this work. The band structure of various isolated nanotubes is presented in Sec. III, and compared to zone-folding of

graphene and tight-binding calculations. In Sec. IV we discuss the band structure of bundles of (10,0), (6,6), and (8,4) nanotubes along the k_z direction and in the perpendicular plane. We compare our results to two selected experiments—STM measurements by Odom *et al.*[5] and Raman scattering by Jorio *et al.*[22]—in Sec. V. Section VI summarizes our work and contains our conclusions.

II. COMPUTATIONAL METHOD

DFT calculations were performed with the SIESTA *ab initio* package.[23] We used the local-density approximation parametrized by Perdew and Zunger[24] and nonlocal norm-conserving pseudopotentials.[25] The valence electrons were described by localized pseudoatomic orbitals with a double-ζ singly polarized (DZP) basis set.[26] Basis sets of this size have been shown to yield structures and total energies in good agreement with those of standard plane-wave calculations.[27] The cutoff radii for the *s* and *p* orbitals were 5.1 and 6.25 a.u., respectively. These radii correspond to a 50-meV energy shift (i.e., an increase in the energy of the electron energy levels by localization in the free atom),[26] which was chosen as the one that minimizes the total energy for a graphene sheet, at the given DZP basis level. Increasing the cutoff of the orbitals only changes the *total* energies of the nanotubes considered here by less than 0.1 eV/atom, and has virtually no effect on the structure and energies of the electronic states. Real-space integration was performed on a regular grid corresponding to a plane-wave cutoff around 250 Ry, for which the structural relaxations and the electronic energies are fully converged. For the total energy calculations of isolated tubes we used between 1 (chiral tubes) and 30 (armchair) *k* points along the k_z direction. The metallic bundles [(6,6) and (10,0) tubes] were sampled by a $10\times10\times30$ Monkhorst-Pack[28] *k* grid; only the Γ point was included for the semiconducting (8,4) nanotube bundle.

For the isolated tube we calculated the theoretical lattice constant and relaxed the atomic coordinates until the forces were below 0.04 eV/Å. For graphene, we obtained a carbon-carbon distance of 1.424 Å. The nanotube radii and translational periodicity agreed to within 1% with the expected values for an ideal cylinder (see Table I in Sec. III and also Table I in Ref. 29). The bundled tubes were relaxed by a conjugate gradient minimization until each component of the stress tensor was below 0.02 GPa and the atomic forces <0.04 eV/Å. The circular cross section of the bundled tubes was slightly hexagonally distorted. The atomic positions of the bundled tubes were used for band-structure calculations of the isolated tubes as well to exclude any effects of polygonization.[30] However, for the (10,0) tube, where the hexagonal distortion was largest (1%), we compared the results obtained with the two sets of atomic coordinates, and found no differences worth mentioning.

The nanotube bundles were constructed from one individual tube placed in the hexagonal bundle unit cell. The wall-to-wall distance between the tubes we calculated as 3.1 Å, slightly smaller than in graphite with the same basis set (3.3 Å). The chosen unit cell always preserves the horizontal mirror plane in achiral nanotubes; additionally, the tubes might be rotated around their *z* axis to yield arrangements of particular high or low symmetry. In the calculations of the (6,6) nanotube bundles we used the highest symmetry packing (D_{6h}). The (8,4) tubes were placed according to D_2 instead of D_{56} in the isolated nanotube. Finally, the (10,0) nanotube bundle was maximally disordered with respect to rotation (C_{2h}, i.e., no vertical planes or horizontal rotation axes).

In the band structure calculations we used 10 to 30 *k* points along the *z* direction for the chiral (8,4) and (10,5) nanotubes, 45 for the zigzag (10,0) and (19,0) nanotubes, and 60 for the armchair (6,6) tube. In the perpendicular direction we included a total of 30 points for the ΓM, MK, and $K\Gamma$ directions. This sampling was sometimes not fully sufficient to describe accurately the crossing of the bands in the interior of the Brillouin zone. We recalculated parts of the Brillouin zone with a finer mesh, and found no level anticrossing when not explicitly stated in the text.[31] Only for one of the tubes discussed in this work were other first-principles band structures available. For the (10,0) tube and graphite we found an excellent agreement with pseudopotential plane-wave calculations.[19,32] We also compared the band structure of the (6,6) armchair tube to the all-electron calculations of Ref. 20, where a series of larger diameter armchair tubes was investigated. The general features are reproduced in our calculations as well.

III. ISOLATED NANOTUBES

In this section we first discuss the band structure of two small achiral nanotubes, paying particular attention to the effects of rehybridization. The calculated band structure of two chiral nanotubes with a diameter $d\approx8$ Å are presented in a separate subsection. Finally, the electronic dispersion in the optical range of a (19,0) tube is investigated.

A. Achiral nanotubes

In Fig. 1(b) we show the band structure of an isolated (10,0) nanotube. Figure 1(a) contains the graphene electronic dispersion folded once along the ΓM direction, and Fig. 1(c) the tight-binding description including only the π orbitals. The dots in Fig. 1(b) indicate nondegenerate bands with quantum number $m=0,n$. The Γ point ($k_z=0$) of the nanotube for these bands corresponds to the Γ and *M* points of graphene, since the perpendicular, quantized wave vector $k_\perp$ is given by $k_\perp=m(\boldsymbol{k}_1/n_1+\boldsymbol{k}_2/2n_1)$ for $(n_1,0)$ zigzag tubes, where $\boldsymbol{k}_1$ and $\boldsymbol{k}_2$ are the reciprocal-lattice vectors of graphene. The wave vector along the nanotube axis is parallel to $\boldsymbol{k}_2$. If the curvature of the nanotube wall is neglected, the band structure of the zigzag tube for the bands corresponding to $m=0,n$ (that is, the nondegenerate bands) would be the same as those of graphene along the Γ-*M* direction [dotted bands in Figs. 1(a) and 1(b)]. Nanotube bands with other *m*'s would also have their counterpart in the graphene band structure, but we will only analyze the comparison of the $m=0,n$ bands for simplicity. Below the Fermi energy the (10,0) electronic dispersion agrees quite well with the confinement picture, in particular in the low energy region. Cor-

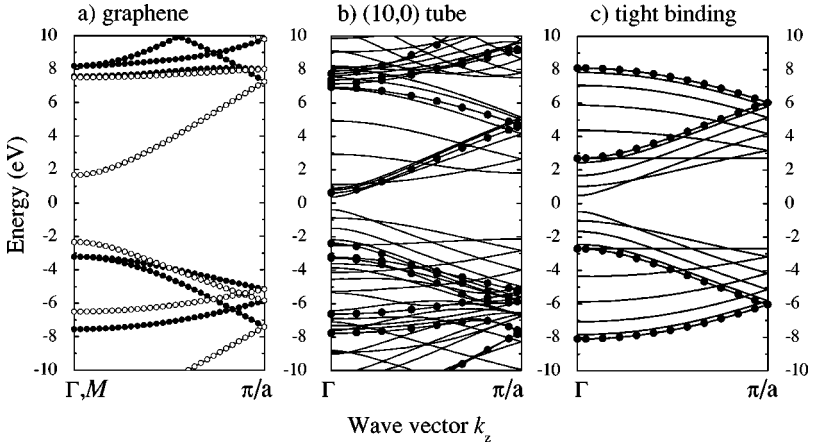

FIG. 1. Band structure of a (10,0) isolated nanotube compared to a zone-folding and tight-binding calculation. (a) *Ab initio* graphene electronic dispersion along the ΓM direction folded at the middle of the Brillouin zone; closed (open) symbols correspond to the first (second) half of the graphene Brillouin zone, i.e., $0 \leq k \leq \pi/3a_0$ ($\pi/3a_0 \leq k \leq 2\pi/3a_0$), where $a_0 = 2.47$ Å is the lattice constant of graphene. (b) *Ab initio* calculation of a (10,0) nanotube. The dots mark the electronic bands with $m = 0,n$ quantum number, which in a zone-folding approximation should have the same dispersion as the graphene band structure shown in (a). (c) Tight-binding calculation of the (10,0) nanotube including only the π orbitals of graphene with $\gamma_0 = 2.7$ eV. The dots indicate the bands with $m = 0,n$. The lattice constant $a = 4.27$ Å in (a), (b), and (c).

respondingly, the tight-binding model, which is adjusted to reproduce the graphite electronic dispersion, gives an adequate description of the nanotube band structure below E_F. The conduction bands, however, are strongly affected by the rolling up of the graphene sheet. It was already pointed out by Blase *et al.*[17] that the rehybridization in small nanotubes shifts the π^* and σ^* bands to lower and higher energies, respectively. The energies of the π^* states in graphene in the (10,0) tube at the Γ point are downshifted by ≈ 1 eV for the $m = n$ and by ≈ 4.4 eV for the $m = 0$ band. While these bands are most strongly affected by the curvature of the tube, others are almost unchanged when comparing Figs. 1(a) and 1(b). In particular, one of the degenerate graphene σ^* bands at 8.14 eV in our calculation is almost at the same energy in the (10,0) nanotube, and shows a similar k dependence. The tight-binding model is not able to reproduce the band structure of the tube above the Fermi level. The differences in energy at the Γ point, which is the critical point from which the singularities in the density of states originate, are vastly exaggerated by omitting the rehybridization (also see Sec. IV).

To study the effect of curvature on the band structure of a nanotube more systematically, in Fig. 2 we show the same calculations for a (6,6) armchair nanotube. The tube's k_z direction is now along the ΓKM line of graphene. The graphene Fermi point at K is thus always included in the allowed states of an armchair tube, making these tubes metallic.[1] When comparing the graphene dispersion to the nondegenerate bands of the (6,6) tube [indicated by the dots in Fig. 2(b)], the overall agreement seems to be much better than for the zigzag tube discussed above. In particular, the folded bands of graphene [see the open symbols in Fig. 2(a)], are almost unaffected by the curvature. Below E_F even the accidental degeneracy of the π bands at the corner of the Brillouin zone is reproduced by the *ab initio* calculations. Nevertheless, above the Fermi level the π^* conduction band is downshifted by 4.7 eV as in the zigzag tube. Table I lists some selected electronic energies in (10,0) and the (6,6) nanotubes, and compares them to the graphene values. The general trend as observed in Figs. 1 and 2 is reflected in the explicit values given in Table I, i.e., (i) the valence bands of carbon nanotubes are well described in a zone-folding ap-

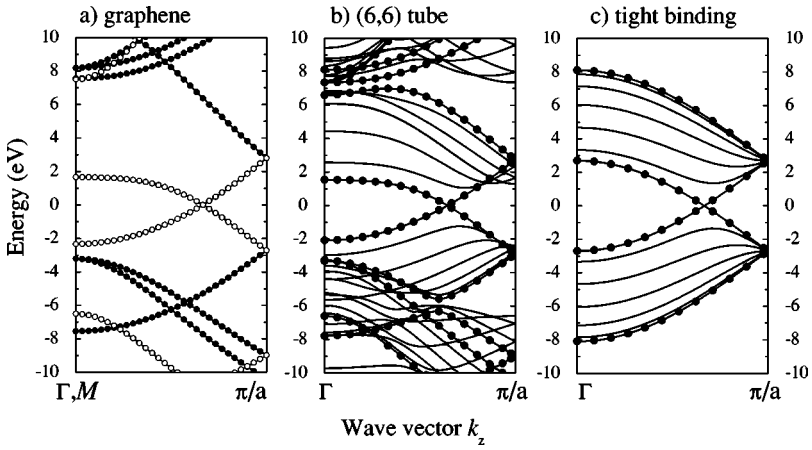

FIG. 2. Band structure of a (6,6) isolated nanotube compared to a zone-folding and tight-binding approximation. (a) Graphene *ab initio* calculation of the band structure along the ΓKM direction folded at $(\boldsymbol{k}_1 - \boldsymbol{k}_2)/4$. Closed (open) symbols correspond to the bands originating at the Γ (M) point of graphene. (b) *Ab initio* calculation of an isolated (6,6) nanotube. The dots indicate the $m = 0,n$ bands, which correspond to the graphene dispersion shown in (a). (c) Tight-binding approximation of the same tube with $\gamma_0 = 2.7$ eV. The lattice constant $a = 2.47$ Å in (a), (b), and (c).

TABLE I. Selected electronic energies at the Γ and *M* points of graphene compared to the Γ-point energies in nanotubes. In a zone-folding approximation the energy difference between graphene and a nanotube is expected to vanish. The twofold degeneracy of the σ^* conduction bands is lifted in carbon nanotubes. The calculated diameter of the nanotubes is given in the second column.

		Conduction				Valence		
		Γ		*M*	Γ		*M*
	d(Å)	π(eV)	σ(eV)	π(eV)	π(eV)	σ(eV)	π(eV)
Graphene		11.3	8.2	1.7	−7.5	−3.2	−2.3
(10,0)	7.8	7.0	10.3 7.7	0.6	−7.8	−3.2	−2.3
(6,6)	8.2	6.6	8.1 10.3	1.5	−7.8	−3.2	−2.1
(8,4)	8.4	6.8	10.3 8.1	1.6	−7.7	−3.2	−2.3
(9,3)	8.5	7.0	10.2 7.9	1.7	−7.8	−3.3	−2.1
(10,5)	10.4	7.2	10.5 8.1	1.6	−7.7	−3.2	−2.3
(19,0)	14.9	7.5	10.2 8.2	1.4	−7.6	−3.2	−2.4

proximation; (ii) for the electronic bands originating from the Γ point of graphene, the upshift of the σ^* and the corresponding downshift of the π^* states is similar for armchair and zigzag tubes with the same radius; and (iii) the conduction bands derived from the graphene *M* point are strongly downshifted in the zigzag tube, whereas they are close to graphene in the (6,6) nanotube.

In Fig. 3 we give an expanded view of the band structure in the energy range of the π^* and σ^* bands at the graphene Γ point; the *x* axis represent 4/10 of the (10,0) and (6,6) Brillouin zones. Full lines show the graphene band structure along the high-symmetry directions; the gray dots are the nondegenerate bands of the (10,0) (left) and (6,6) (right) nanotubes. The graphene bands are labeled by their irreducible representations at the Γ point and along the Γ*M* direction for the zigzag tube, and the Γ*K* direction for the armchair tube. In this picture the graphene dispersion was not folded to keep the figure as simple as possible. In the enlarged picture it is apparent that, e.g., the Γ_2^+ state and one of

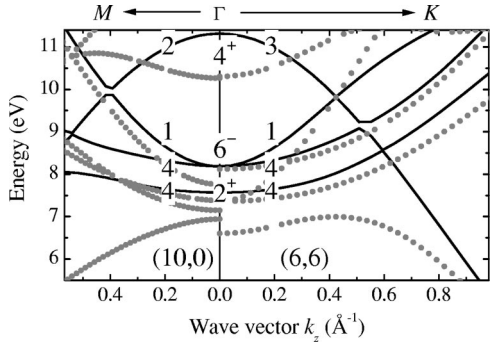

FIG. 3. Electronic dispersion of graphene (full lines) around the Γ point in the energy range of the lowest-lying conduction bands. The Γ*M* direction is displayed to the left together with the nondegenerate bands in a (10,0) nanotube (gray dots). To the right the Γ*K* electronic dispersion of graphene and the nondegenerate bands of a (6,6) armchair tube (gray dots) are shown. The irreducible representations of the graphene electronic bands are given in Slater's notation (Ref. 33).

the bands forming the degenerate Γ_6^- state in graphene have similar energies and dispersions in graphene and in the tubes. In contrast, the Γ_4^+ band (π^*) and the second Γ_6^- state are shifted by the rehybridization. To understand this different behavior, let us consider the symmetry lowering by cutting a graphene sheet and rolling it up to a nanotube. By doing so we lose all rotations by angles other than 180° and all operations changing the graphene *z* coordinate like σ_h or the primed rotations. In achiral nanotubes we preserve reflections perpendicular to the *x* and *y* axes. This is a somehow local description of the symmetry of a curved sheet, since the point groups of nanotubes involve translational symmetry operations of graphene.[31] For the present purpose, however, this picture is sufficient. In the lower symmetry group Γ_6^- and Γ_4^+ belong to the same representation which is different from the original Γ_2^+ irreducible representation. A mixing and band repulsion can thus be expected for the two former bands. In the interior of the Brillouin zone T_1 and T_3 (along the Γ*K* direction) and Σ_2 and Σ_4 (Γ*M*) are correlated with the same representation. The behavior as expected by symmetry is nicely seen in Fig. 3. At the Γ point the 2^+ state is pinned at its graphene energy, whereas a mixing and band repulsion is obvious for the 4^+ and 6^- states. The mixing is only found for the Σ_4 and the T_1 band in the zigzag and armchair nanotube, respectively, as predicted. In the (10,0) nanotube the symmetry analysis given so far is valid for all k_z, and the π conduction band as a whole is expected to be downshifted. In armchair nanotubes, after passing, *K*-point mixing is forbidden by symmetry even for the bent sheet for the bands within ≈10 eV of the π^* states. Their electronic energies corresponding to the graphene *M* point are thus more weakly affected by band repulsion, as we found in the *ab initio* calculations.

B. Chiral nanotubes

In Table I we include the electronic energies of the calculated (n_1,n_2) chiral nanotubes corresponding to the Γ and *M* point of graphene. Both high-symmetry points are always allowed states in carbon nanotubes. For the Γ point this is trivial, while for the *M* point it can be understood in the following way. Consider a graphene wave vector pointing in the direction of the nanotube circumferential, quantized wave vector,

$$k_\perp = \frac{2n_1+n_2}{qn\mathcal{R}}\boldsymbol{k}_1 + \frac{2n_2+n_1}{qn\mathcal{R}}\boldsymbol{k}_2, \tag{1}$$

where *n* is the greatest common divisor of n_1 and n_2, $\mathcal{R}=3$ if $(n_1-n_2)/3n$ integer and $\mathcal{R}=1$ otherwise, and *q* is the number of graphene hexagons in the unit cell of the nanotube.[15] The graphene points in reciprocal space corresponding to the Γ point of the nanotube are given by $k_\Gamma = mk_\perp$ (*m* integer and $-q/2<m\leqslant q/2$). Let us assume that we are dealing with a $\mathcal{R}=1$ nanotube. The Γ point of the band with $m=q/2$ is then given by

$$k_\Gamma(q/2) = \frac{1}{n}\left(\frac{2n_1+n_2}{2}\boldsymbol{k}_1 + \frac{2n_2+n_1}{2}\boldsymbol{k}_2\right)$$

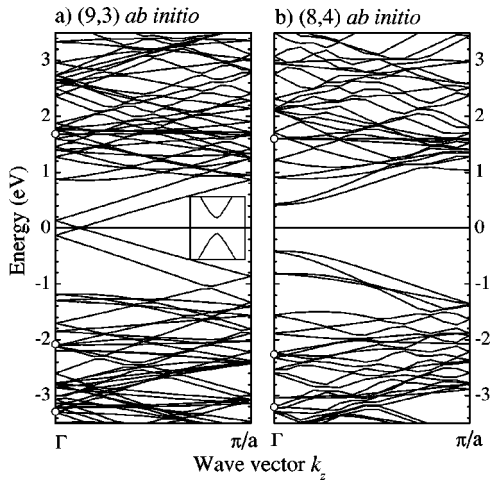

FIG. 4. *Ab initio* band structure of two chiral nanotubes. (a) (9,3) quasimetallic nanotube ($a=15.44$ Å). The inset (vertical scale ± 35 meV) shows the secondary gap at the Fermi level evolving because of the curvature of the nanotube wall. (b) (8,4) semiconducting nanotube ($a=11.30$ Å). The open dots in (a) and (b) indicate the energy of the nondegenerate states at the Γ point; see Table I

$$= \boldsymbol{G} + \frac{1}{n}\left(\frac{n_2}{2}\boldsymbol{k}_1 + \frac{n_1}{2}\boldsymbol{k}_2\right), \tag{2}$$

where $\boldsymbol{G}$ is a reciprocal-lattice vector of graphene. The possible solution of Eq. (2) after subtracting reciprocal-lattice vectors are $\boldsymbol{k}_1/2$, $\boldsymbol{k}_2/2$, and $(\boldsymbol{k}_1+\boldsymbol{k}_2)/2$. All three yield the *M* point of graphene. For the tube with $\mathcal{R}=3$ the same can be proven by using the condition that $(n_1-n_2)/3n$ is an integer. Therefore we can—as in achiral nanotubes—directly compare the graphene electronic energies to the *ab initio* calculations of the chiral nanotubes to estimate the effect of hybridization. As can be seen in Table I, the curvature-induced shift of the nondegenerate bands is of similar magnitude in chiral and achiral nanotubes of similar diameters. For the π^* band originating from the Γ point of graphene, the achiral tubes seem to indicate the two limiting cases with the strongest downshift in the (6,6) armchair and the weakest in the (10,0) zigzag tube. However, neither of the two chiral tubes exhibits large differences from the zone-folding approximation for the bands derived from the *M* point of graphene. The (10,0) zigzag tube is clearly singled out here compared to chiral or armchair tubes.

The full electronic dispersion for (9,3) and (8,4) nanotubes is shown in Figs. 4(a) and 4(b), respectively. In the inset in Fig. 4(b) the secondary gap of 20 meV can be seen induced in the (9,3) nanotube by curvature. The magnitude of the band gap is smaller than recently estimated by Kleiner and Eggert,[34] who considered the geometric effect of hybridization on the secondary gap. Using their relation we find a band gap on the order of 100 meV. The discrepancies might partly be due to the usual local-density-approximation (LDA) problem of underestimating gap energies and partly to the band repulsion which was not considered by Kleiner and Eggert.[34]

The energies of the next highest valence and conduction bands at the Γ point are remarkable asymmetric with respect to the Fermi level. The asymmetry is particularly pronounced in the (9,3) nanotube, but visible in the (8,4) tube as well. Two reasons account for the different behaviors below and above the Fermi level. First, the graphene electronic dispersion is slightly different for the valence and conduction bands. Second, the higher bands move toward the Fermi level because of the curvature. For example, in the (8,4) tube the third singularities below and above E_F are within zone folding at -1.59 and 1.45 eV. In the *ab initio* calculation of the tube the valence energy is approximately the same as in the zone-folding calculation, whereas the conduction band is further lowered and has an energy of 1.22 eV in Fig. 4(b). A very similar shift is observed for the first singularity in the (9,3) tube; again the valence-band energies are the same, while we find a difference of 0.20 eV between the zone-folded and *ab initio*-calculated conduction band. Note that these singularities are usually probed by optical experiments; they are responsible for the resonant Raman scattering in the red (metallic resonance) and blue energy ranges.

C. Diameter dependence

Up to now, we considered only nanotubes with small diameters. In this section we discuss the band structure of a (19,0) nanotube which has a diameter more typical of real nanotube samples ($d=14.9$ Å). We selected a zigzag tube, because, as we showed in Sec. III B, the hybridization effects are largest for these tubes. The (19,0) nanotube, in this sense, serves as a worst case scenario for judging how strongly curvature influences the band structure of real nanotubes.

Although the curvature of the (19,0) nanotube is considerably smaller than that of the (10,0) nanotube or any other nanotube discussed so far, we still find a downshift of the π^* band at the Γ point of 3.8 eV and an upshift of one of the σ^* states by 2 eV (see Table I). These two values are not so much different from the small diameter nanotubes as might be expected. As we discussed in Sec. III A this can be understood by the lower symmetry in a curved sheet. The difference in energy between the zone-folding approximation and the *ab initio* calculation for the nondegenerate band originating from the *M* point of graphene, however, is much reduced in the (19,0) tube (0.3 eV) when compared to the (10,0) nanotube (1.1 eV).

In Fig. 5 we present the band structure within 2 eV around the Fermi level, i.e., in the optical energy range where many experiments have been performed. Figure 5(a) shows the conduction bands labeled by their *m* quantum numbers; in Fig. 5(b) the valence bands are displayed [the *y* scale is negative in Fig. 5(b)]. The gray dots indicate the position of the electronic states at the Γ point obtained within the zone-folding approximation from the *ab initio* calculation of graphene. Below the Fermi level zone folding very nicely describes the first-principles results. For the conduction bands with $m=14$ and 15, clear deviations are seen. This is easily understood, since in a zigzag tube the bands with $m \geqslant q/3$ have a $k_\perp$ which is on the line between the *K* and the *M* point in graphene, see Eq. (2). The energy of the *M* point

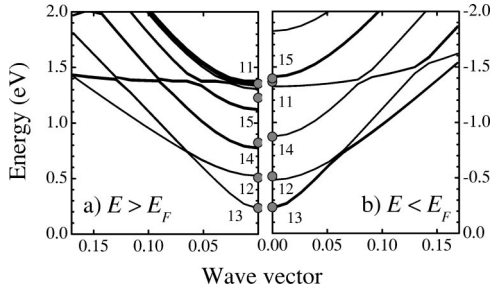

FIG. 5. Band structure in the optical energy range of a (19,0) nanotube by first-principles calculation. (a) Conduction bands within 2 eV of the Fermi level. The labels indicate the m quantum numbers of the conduction bands; $m=11$ refers to the second-lowest band in energy in the group of bands at 1.34 eV (Γ point). The other bands with a Γ point energy ≈ 1.34 eV have quantum numbers between $m=16$ and 19 (not explicitly labeled in the figure). (b) Same as (a), but for the valence bands. The gray dots show the zone-folding electronic energies at the Γ point.

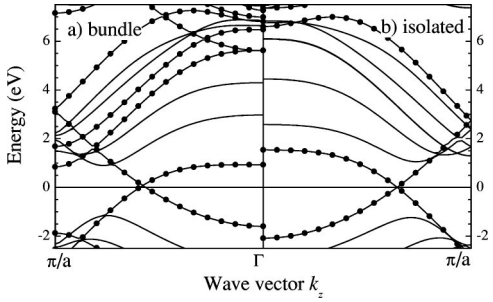

FIG. 6. Dispersion along the k_z axis for (a) a bundle of (6,6) armchair tubes, and (b) the isolated armchair tube. Nondegenerate bands are indicated by the closed dots. The Fermi level which is at -5.79 eV in the bundle, but -5.12 eV in the single tube was set to zero. Note that the crossing of the valence and conduction bands occurs slightly (70 meV) above the Fermi level at the Fermi wave vector $k_{zF}=0.73$ Å$^{-1}=0.57\pi/a$.

is most strongly changed by the hybridization in the (19,0) nanotube and, hence, the closer the confinement wave vector is to M the larger the expected energy shift. In the present example, $k_\perp \approx 0.2KM$ and $0.4KM$ for a band with $m=14$ and 15, respectively. Bands with an m quantum number between 16 and 19, together with the $m=11$ band form the group of bands at 1.34 eV in Fig. 5(a).

An interesting point arises when we fit the electronic energies E_m at the Γ point by the tight-binding approximation to test its validity. For zigzag tubes at $k_z=0$ the energies are given by[15]

$$|E_m| = \gamma_0(1+2\cos m\pi/n). \tag{3}$$

The γ_0 we obtain increases monotonically from 2.4 to 2.6 eV between $m=13$ and 11 (the $m=15$ band shown in Fig. 5 has again a lower value). STM studies often concentrated on the lowest singularities in the density of states, while optical experiments are sensitive to the bands higher in energy. This increase in γ_0 is probably one reason for the smaller overlap integral found in STM compared to Raman experiments.

IV. BUNDLED NANOTUBES

A bundling of the nanotubes to ropes induces further changes in the electronic dispersion along the tubes axis. The most prominent example is the opening of a pseudogap in armchair nanotubes.[8,21] We also discuss the differences for the higher valence and conduction bands before turning to the dispersion perpendicular to the z axis.

A. Dispersion along k_z

In Fig. 6(a) we show the band structure of a bundle of (6,6) armchair tubes and that of an isolated tube in Fig. 6(b). The nondegenerate states in both figures are indicated by small dots. When comparing bundled and isolated nanotubes, a number of differences are apparent: (i) the first valence and conduction bands cross slightly above the Fermi level (70 meV) in the bundles of tubes; (ii) a further shift of the valence bands is observed, which is most pronounced for the nondegenerate bands; and (iii) one of the doubly degenerate states in the isolated tubes splits in the bundle.

At first sight it might seem surprising that we do not obtain a secondary band gap in the nanotube bundles, but—as pointed out by Delaney *et al.*[7,8]—this is simply due to the high-symmetry configuration we used for the bundles. We arranged the (6,6) tubes in a hexagonal lattice which fully preserves the D_{6h} symmetry of the hexagonal packing, i.e., half of the original mirror symmetries perpendicular to the z axis are also symmetry operations of the bundles. The electronic wave functions can still be classified as even or odd with respect to these reflections, allowing a crossing of the two bands at high-symmetry lines in the Brillouin zone.[7,8] Another example of such a crossing is seen at 7 eV, roughly in the middle of the Brillouin zone, in Fig. 6(a). The π^*-derived band, which has an odd parity under σ_v crosses with one of the σ^* bands; the latter is downshifted by interactions between the tubes. The two newly obtained nondegenerate bands in the bundles of armchair tubes (Γ point energy 5.60 and 6.46 eV) originate from the doubly degenerate bands with the quantum number $m=3$ (6.10 eV). In the new point group they are correlated with the B_1 and B_2 representations ($_kE_{A_n}$ and $_kE_{B_n}$ in the line group notation).[15] Likewise, m and $(6-m)$ now belong to the same representation, which opens up small gaps at the zone boundary. The compatibility between the nanotube symmetry group and the hexagonal packing is, however, a special case, because D_{6h} is a subgroup of the (6,6) tube. In general, the symmetry is at least reduced to D_{2h} for achiral tubes and D_2 for chiral tubes, even in the highest symmetry configuration. These groups have only nondegenerate representations, and hence the degeneracy will be lifted for all bands in a general tube, when it is bundled. An interesting question is how strongly the bundle band structure, in particular that perpendicular to k_z, depends on the relative orientation of the tubes. The calculations by Delaney *et al.*[7,8] showed only a weak dependence of the density of states in armchair bundles on tube rotation. To break the D_{6h} symmetry of the (6,6) bundle, we rotated the tubes within the unit cell by 5°. For this arrangement we calculated the band structure along the k_z direction without further structural relaxation.[35] The small rotation opened up

TABLE II. Critical-point energies around the Fermi level. The table compares results of the zone-folding approximation including only the π orbitals of graphene (π orbitals, $\gamma_0 = 2.7$ eV), zone folding of the graphene band structure calculated with SIESTA (folding), the *ab initio* result of an isolated tube [*ai* (single)], and the *ab initio* calculation of bundles of tubes [*ai* (bundle)]. For the bundle the mean value for split bands was given; when the splitting was >0.1 eV, we included the splitting in parentheses. For each tube the rows are ordered by the energies of the tight-binding approximation for the graphene π orbitals.

Tube	$\|m\|$	Electronic energies at critical points (eV)							
		π orbitals	folding	*ai* (single)	*ai* (bundle)	π orbitals	folding	*ai* (single)	*ai* (bundle)
(6,6)	5	1.35	1.13	1.05	0.89	−1.35	−1.24	−1.23	−1.16
	6	2.34	1.58	1.34	1.27	−2.34	−2.06	−2.07	−2.13
(10,0)	7	0.47	0.43	0.38	0.43 (0.21)	−0.47	−0.44	−0.37	−0.35 (0.37)
	6	1.03	1.00	1.12	0.84 (0.14)	−1.03	−1.01	−0.87	−0.99 (0.45)
	8	1.67	1.28	0.80	0.47 (0.21)	−1.67	−1.49	−1.48	−1.87
(8,4)	19	0.45	0.42	0.43	0.40	−0.45	−0.42	−0.43	−0.38
	18	0.95	0.90	0.90	0.64	−0.95	−0.92	−0.92	−0.92
	20	1.70	1.45	1.22	0.96	−1.70	−1.59	−1.53	−1.77

the secondary gap at the Fermi level (51 meV), as expected. Additionally, the energy of the first singularity of the conduction bands was higher by 60 meV in the less symmetric arrangement, whereas the effect was small for the higher conduction bands. The valence bands were hardly affected by the rotation. A systematic study of the band structure and its orientation dependence in bundles of different chirality will be the subject of a future work.

The bundling moves the Γ point energies of the lowest valence and conduction bands in the (6,6) nanotubes closer to the Fermi level. In contrast to isolated tubes, the bundling shifts the two bands by the same order of magnitude (-0.62 eV for the conduction and 0.48 eV for the valence band). In Sec. III C we saw that the change in the *M*-point energy is indicative of the Γ-point energies of the other bands and the densities of electronic states. We therefore might expect a similar change in the electronic dispersion for other bundles as well. In Table II we summarize the energies at critical points in the Brillouin zone, which we obtained by different calculations. We included only the first three bands around the Fermi level within the tight-binding approximation using the π orbitals of graphene. The intertube coupling induces a shift of the valence- and conduction-band singularities, which might be as high as 0.25 eV in the (6,6) and (8,4) nanotube. The (10,0) nanotube is somewhat peculiar because of the strong splitting of its bands. Note that the valence and conduction bands originating from the $m=7$ band in the isolated tube are only separated by 0.2 eV in the bundle, compared to 0.75 eV for the single tube. Moreover, the highest valence band is 0.02 eV above the Fermi level at the Γ point (see Sec. IV B).

Rao *et al.*[36] recently reported a parametrized calculation of isolated and bundled armchair nanotubes using the method of Kwon *et al.*[21] They observed differences of similar magnitude in the density of states in isolated and bundled tubes, but—in contrast to us—an increase in the separation of the valence- and conduction-band singularities. This discrepancy is partly due to our assumption that the points of vanishing slopes in the band structure reflect the density of states in the bundled tube (the van Hove singularities are broadened in the bundle). On the other hand, the band structures calculated by Kwon *et al.*[21] with a parametrized technique underestimate the differences between single tubes and bundles compared to *ab initio* calculations. Rao *et al.*[36] used the separation between the singularities in the valence and conduction bands to analyze the optical absorption in bundles of carbon nanotubes. For armchair nanotube bundles, however, this analysis includes indirect optical transitions, which are unlikely to occur [see the points of vanishing slopes in Fig. 6(a)]. A more detailed study should consider at least the joint density of states if not the optical transition matrix elements. STM measurements revealed no shift in the first singularity of the density of electronic states between an isolated armchair tube and the same nanotube on top of a bundle, while the second singularity below E_F is slightly at lower energies in the ''bundled'' tubes.[6] Nevertheless, it would be interesting to repeat these measurements for small semiconducting zigzag tubes, which we found to be much more sensitive to the intertube interaction.

B. Intratube dispersion

The interaction between nanotubes in a bundle does not only alter the k_z band structure, but causes a dispersion in the perpendicular plane as well. In graphite the intralayer dispersion for the π bands is ≈ 1 eV and below; the strongest dispersion is found for the σ^* states along the ΓA direction (3–4 eV).[19] The band structure of bulk C_{60} was investigated by Troullier and Martins,[18] who reported bandwidths of around 0.5 eV.

In Fig. 7 we show the band structure of a bundle of (6,6) armchair tubes along several high-symmetry lines in the hexagonal Brillouin zone. The panel to the right shows the perpendicular dispersion at the Fermi wave vector along the *z* axis Δ_F. The secondary gap in the bundled tube is very clearly seen. We obtain the largest separation at the *P* point of the Brillouin zone $\Delta E = 1.2$ eV. Also note the crossing of the two bands with $m=3$ quantum numbers in the isolated

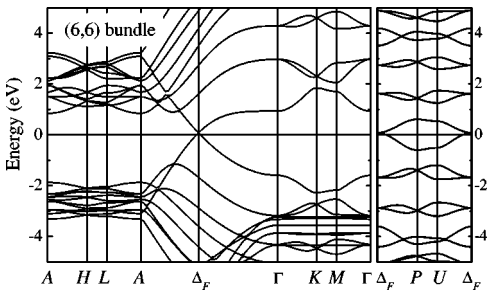

FIG. 7. Band structure of a bundle of (6,6) nanotubes along several high-symmetry lines in the hexagonal Brillouin zone. The right panel shows the intratube dispersions at the Fermi wave vector $k_{zF}=0.73$ Å^{-1} in this calculation.

tube [see the dotted lines in Fig. 6(a), and the discussion in the text] around ± 4 eV. The bandwidths we obtained perpendicular to the z direction are typically between 400 and 600 meV, but might be as high as 900 meV for the two first valence bands at the ΓKM line. The perpendicular dispersion leads to a broadening of the density of states in bundled tubes. Similarly, the broad and unstructured features found in absorption experiments[12,13] on bundled nanotubes might already be expected from the band structure of a bundle composed of a single nanotube species with one important exception: the first optical transition E_{11} coming from the accidental singularities along the ΓA direction of the Brillouin zone falls into the gap of all other vertical excitations. Optical transitions at k points with $k_z=0$ are forbidden in isolated armchair nanotubes, and will be weak or absent in bundled tubes as well;[15] all other transition energies are clearly different in energy from E_{11}. We can take the armchair tubes to be representative of metallic tubes with $\mathcal{R}=3$, which refers to almost all metallic tubes for large enough diameters ($d \gtrapprox 1.2$ nm). Chiral tubes with $\mathcal{R}=3$ have a band structure very similar to armchair tubes; in particular, they possess the same accidental critical point.[37,38] In Raman-scattering experiments, the resonances for the first transition in metallic nanotubes are, therefore, expected to be much more pronounced than the semiconducting resonances, where a similar optical gap is not present (see below). This is in very good agreement with Raman experiments on bundled tubes.[9,10,39] Rafailov *et al.*[10] normalized their measurements to a reference crystal. Indeed, the scattering by metallic nanotubes is very weak outside a well-defined resonance window (1.6–2.0 eV), whereas a comparatively strong signal from the semiconducting nanotubes is found even in the red energy range where they are not expected to be resonant.

In Fig. 8 we show the band structure of a bundle composed of (10,0) nanotubes. The dispersion of the electronic bands perpendicular to k_z is less than in armchair nanotubes; most of the bands have a widths well below 400 meV. The large splitting of the first two valence states at the Γ point and of both conduction and valence bands at the A point of the Brillouin zone results in a stronger dispersion of the corresponding states perpendicular to k_z as well (0.4–0.9 eV). The most interesting point in Fig. 8 is, however, the dispersion of the lowest conduction and the highest valence band in the ΓKM plane. The conduction band—bending down

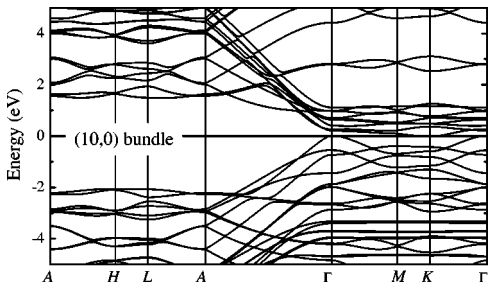

FIG. 8. Band structure of a bundle of (10,0) nanotubes. The two valence bands next to the Fermi energy are strongly split by the tube intertube interaction. Note that the first conduction band is below the Fermi level at the K point of the hexagonal Brillouin zone.

when going away from the Γ point within the plane—crosses the Fermi level close to the K point of the Brillouin zone. Its minimum at K has an energy of -0.02 eV. The highest valence band has a hole pocket at the Γ point (0.02 eV). We thus find the (10,0) nanotube bundle to be metallic in our calculation. A reduction of the band gap by intratube interaction is observed in the (8,4) nanotube bundle as well (see Fig. 9). Again the lowest valence band bends down along the ΓKM line with a minimum at K (0.27 eV). The minimum is still above the Fermi level, because the energy at the Γ point in the (8,4) nanotube is considerably higher than in the (10,0) tube and the intratube dispersion narrower (0.13 eV instead of 0.23 eV). In general, the band gap of nanotubes scales as the inverse of the diameter. If the intratube dispersion is on the same order in larger diameter tubes, the spanning of the gap by the interaction between the tubes is expected to occur as well. At present, we have no calculation for bundles composed of nanotubes with a diameter above 8 Å, which might be addressed in a future work.

The dispersion we find in the chiral (8,4) nanotube bundle in Fig. 9 is again reduced when compared to the zigzag tube bundle in Fig. 8. Only rarely have we found a bandwidth larger than 200 meV. We also stress that in the energy range corresponding to excitations in the visible the (8,4) bundles show a rich band structure in the AHL plane. This might considerably broaden the absorption bands, as discussed above.

V. COMPARISON TO EXPERIMENTS

In this section we compare our calculation to STM and Raman experiments. We show that indeed the discrepancies

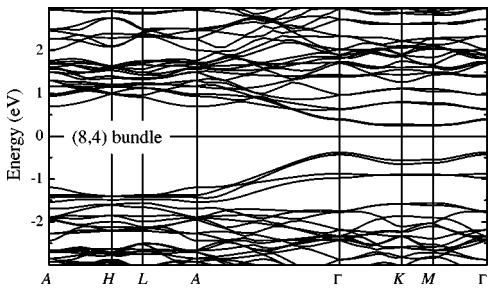

FIG. 9. Band structure of a bundle of (8,4) chiral nanotubes. The x axis between the Γ and A points was expanded by a factor of 3.

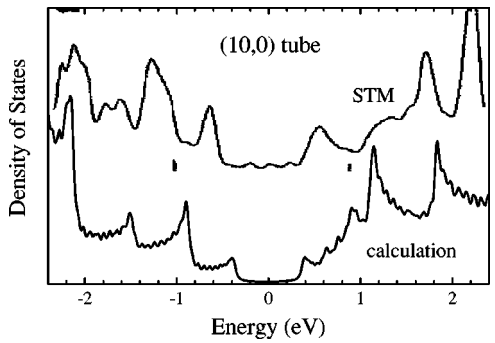

FIG. 10. Density of states measured by scanning tunneling microscopy (top) and calculated with SIESTA. Our calculations reproduce the main features of the experimental density of states, in particular the relative heights of the peaks as is discussed in the text. The energy gap is underestimated by the LDA calculation. The STM data are from Ref. 5

observed between the STM measurement and the density of states above E_F within the tight-binding picture are due to the rehybridization as suggested by Odom *et al.*[5] A reliable energy for optical transitions cannot be obtained from the π-orbital tight-binding Hamiltonian.

A. Scanning tunneling microscopy

STM experiments provide the unique possibility of measuring the density of states on a nanotube of known chirality. Thus they allow a direct comparison between first-principles calculation and experiments. A variety of STM measurements on atomically resolved single-walled nanotubes were reported.[3–5,40,41] Odom *et al.*[5] measured the density of states on a (10,0) nanotube, one of the tubes calculated in this work.

We compare the experimentally obtained density of states of a (10,0) nanotube to our calculation in Fig. 10. The shape and relative height of the peaks are in very good agreement between experiment and theory. In particular, the low-energy shoulder of the second peak above the Fermi level and the much lower height of the third peak below E_F are very nicely reproduced. The absolute energies of the peaks, on the other hand, are considerably smaller in the *ab initio* calculation than in the experimental spectrum. Li *et al.*[42] recently reported similar discrepancies between experiment and theory for very small nanotubes ($d=4$ Å). Their LDA calculations underestimated the optical transition energies by 10–15 %. Also note that the relative energies of the σ and π valence bands in graphite were incorrectly predicted by *ab initio* methods.[19] However, when comparing the absolute peak positions in the upper and lower traces in Fig. 10, the differences are too large to be attributable to the local-density approximation. On the other hand, the calculations still show a very sharp onset of singularities, whereas the experimental curve is much smoother. When we compare the onsets of the flanks rather than the maxima of the peaks, the calculated energies are only 10–20 % too small, which is a typical value for a LDA calculation and was also found by Li *et al.*[42]

B. Raman scattering

Raman scattering is widely used to study the electronic structure of carbon nanotubes by resonant transitions. For bulk samples the approximation of Mintmire and White[1] was successfully used to model the absorption of an ensemble of tubes with a homogeneous chirality distribution.[9,10] The resonant enhancement of the radial breathing mode was also measured on a single tube using a variable excitation energy.[11] The width of the resonance window was reported to be ≈ 10 meV, much smaller than found in tunneling experiments. The disadvantage of Raman scattering, however, is the unknown chirality of the scattering nanotube. Recently, attempts were made to determine not only the diameter, but also the chirality of a nanotube by Raman scattering.[22,43] To identify possible tubes resonant with the incoming or outgoing photons, both groups used the tight-binding approximation of the graphene π orbitals with $\gamma_0=2.9$ eV, as found on nanotube bundles. Within this model the dependence of the electronic energies on chirality arises mainly from the trigonal shape of the energy contours around the graphene K point.[14,16] By comparing the intensities of the radial breathing modes coming from a number of different tubes, they adjusted the dependence of the breathing mode on the diameter until they found good agreement between the expected and observed intensities. The chirality assignment thus relied heavily on the assumed transition energies. The question arises of whether this is indeed a reliable procedure to identify a particular (n_1,n_2) nanotube.

To study this question we selected the semiconducting (10,5) nanotube, which Jorio *et al.*[22] assigned on the basis of Raman data. We calculated the electronic density of states with the tight-binding approximation of the graphene π orbitals, zone folding of a graphene sheet, and by a first-principles calculation. The optical transition investigated in the Raman study corresponds to the $m=\pm 24$ quantum number in the (10,5) nanotube.[15] In Fig. 11 we compare the density of states obtained by the three models for this particular band. We found the energetic position of the valence-band singularity within zone folding to be the same as in the full calculation of the (10,5) nanotube. We therefore adjusted the tight-binding approximation to yield the same energy ($\gamma_0=2.54$ eV). The upper scale corresponds to a tight-binding parameter $\gamma_0=2.9$ eV, which was found on bundles of nanotubes. Using the upper scale to compare our calculations directly to the work by Jorio *et al.*,[22] we find a transition energy of 1.54 eV in the tight-binding approximation. This energy was within the resonance window in Ref. 22 between 1.48 and 1.68 eV. Already the zone-folding calculation shows a smaller separation of the valence- and conduction-band singularities. From an *ab initio* calculation of the (10,5) nanotube we obtain a transition energy 1.44 eV, clearly outside the resonant range. Note that the difference between the *ab initio* and tight-binding calculations is twice as much as the trigonal shape corrections (50 meV). The error made when using the tight-binding approach thus makes it impossible to use resonances for the assignment of chiralities to particular nanotubes.

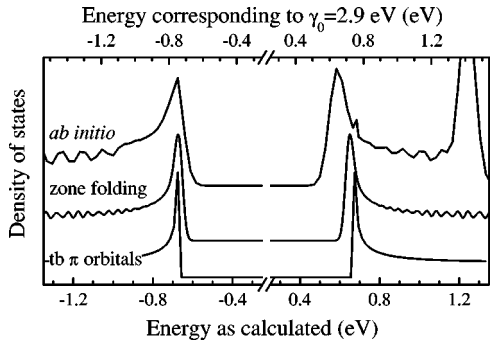

FIG. 11. Density of states in a (10,5) nanotube for the band with quantum number $m=\pm 24$. From bottom to top we show the singularities obtained with the tight-binding approximation (π orbitals only), the zone folding of the graphene band structure, and an *ab initio* calculation. The bottom x scale is for energies obtained from first-principles calculations for a (10,5) nanotube and graphene; within the tight-binding calculation the overlap parameter was adjusted to yield the same energetic position for the singularity below E_F as in the first-principles calculation ($\gamma_0=2.54$ eV). The top scale corresponds to $\gamma_0=2.9$ eV; it might be considered to be corrected for too small a band gap in the LDA approximation.

VI. SUMMARY

We calculated the electronic band structures for isolated and bundled carbon nanotubes, and compared them to zone-folding and tight-binding calculations. In the isolated tubes we paid particular attention to the hybridization of the π and σ orbitals of graphene, which are induced by the curvature of the nanotube wall. Whereas the valence bands and the low-energy conduction bands ($E<1.0$ eV) are very well reproduced by a zone-folding approximation, deviations on the order of 200 meV were found for the conduction bands involved in optical transitions. Zigzag nanotubes are particularly sensitive to hybridization effects; even in a (19,0) nanotube the energy band derived from the π conduction band at the graphene M point is downshifted by 0.3 eV.

We studied the effect of bundling on the electronic states on two achiral nanotubes and a chiral nanotube. For many bands a further shift of the Γ-point energies toward the Fermi level on the order of 100 meV was observed. In the semiconducting bundles we found an intramolecular dispersion of the lowest conduction band, bending down when going away from the Γ point. In chiral (8,4) tubes the band gap was thereby reduced by 20 % compared to the isolated case, whereas the (10,0) nanotube bundle turned out to be metallic. The electronic dispersion perpendicular to the tubes was found to range from ≈ 200 meV in chiral tubes to 1 eV in armchair nanotubes, which is expected to broaden the density of states as well as optical-absorption bands in nanotube bundles.

Finally, we investigated the validity of the tight-binding approximation of graphene π orbitals by comparing its results to first principles calculations. In general, the agreement between the two calculations was found to be satisfactory. However, the simple tight-binding model is certainly not suited to predict electronic energies with an accuracy of 100 meV, as assumed recently in the interpretation of Raman scattering experiments.

ACKNOWLEDGMENTS

We thank X. Blase for sending us his plane-wave calculation of a (10,0) nanotube, and J. Maultzsch for helpful discussions. We acknowledge the Ministerio de Ciéncia y Technología (Spain) and the DAAD (Germany) for a Spanish-German Research action (HA 1999-0118). P. O. acknowledges support from Fundación Ramón Areces (Spain), EU Project No. SATURN IST-1999-10593, and Spain-DGI Project No. BFM2000-1312-002-01. Parts of this work were supported by the Deutsche Forschungsgemeinschaft under Grant No. Th 662/8-1.

[1] J.W. Mintmire and C.T. White, Phys. Rev. Lett. **81**, 2506 (1998).
[2] C.T. White and J.W. Mintmire, Nature (London) **394**, 29 (1998).
[3] J.W.G. Wildöer, L.C. Venema, A.G. Rinzler, R.E. Smalley, and C. Dekker, Nature (London) **391**, 59 (1998).
[4] T.W. Odom, J.L. Huang, P. Kim, and C.M. Lieber, Nature (London) **391**, 62 (1998).
[5] T.W. Odom, J.-L. Huang, P. Kim, and C.M. Lieber, J. Phys. Chem. B **104**, 2794 (2000).
[6] M. Ouyang, J.-L. Huang, C.L. Cheung, and C.M. Lieber, Science **292**, 702 (2001).
[7] P. Delaney, H.J. Choi, J. Ihm, S.G. Louie, and M.L. Cohen, Nature (London) **391**, 466 (1998).
[8] P. Delaney, H.J. Choi, J. Ihm, S.G. Louie, and M.L. Cohen, Phys. Rev. B **60**, 7899 (1999).
[9] M.A. Pimenta, A. Marucci, S.A. Empedocles, M.G. Bawendi, E.B. Hanlon, A.M. Rao, P.C. Eklund, R.E. Smalley, G. Dresselhaus, and M.S. Dresselhaus, Phys. Rev. B **58**, R16 016 (1998).
[10] P.M. Rafailov, H. Jantoljak, and C. Thomsen, Phys. Rev. B **61**, 16 179 (2000).
[11] A. Jorio, A.G.S. Filho, G. Dresselhaus, M.S. Dresselhaus, R. Saito, J.H. Hafner, C.M. Lieber, F.M. Matinaga, M.S.S. Dantas, and M.A. Pimenta, Phys. Rev. B **63**, 245416 (2001).
[12] O. Jost *et al.*, Appl. Phys. Lett. **75**, 2217 (1999).
[13] J. Hwang, H.H. Gommans, A. Ugawa, H. Tashiro, R. Haggenmueller, K.I. Winey, J.E. Fischer, D.B. Tanner, and A.G. Rinzler, Phys. Rev. B **62**, R13 310 (2000).
[14] R. Saito, G. Dresselhaus, and M.S. Dresselhaus, Phys. Rev. B **61**, 2981 (2000).
[15] M. Damnjanović, T. Vuković, and I. Milošević, J. Phys. A **33**, 6561 (2000).
[16] S. Reich and C. Thomsen, Phys. Rev. B **62**, 4273 (2000).
[17] X. Blase, L.X. Benedict, E.L. Shirley, and S.G. Louie, Phys. Rev. Lett. **72**, 1878 (1994).
[18] N. Troullier and J.L. Martins, Phys. Rev. B **46**, 1754 (1992).
[19] M.C. Schabel and J.L. Martins, Phys. Rev. B **46**, 7185 (1992).
[20] J. Mintmire and C.T. White, Appl. Phys. A: Solids Surf. **67**, 65 (1998).

[21] Y.-K. Kwon, S. Saito, and D. Tománek, Phys. Rev. B **58**, R13 314 (1998).
[22] A. Jorio, R. Saito, J.H. Hafner, C.M. Lieber, M. Hunter, T. McClure, G. Dresselhaus, and M.S. Dresselhaus, Phys. Rev. Lett. **86**, 1118 (2001).
[23] D. Sanchez-Portal, P. Ordejón, E. Artacho, and J.M. Soler, Int. J. Quantum Chem. **65**, 453 (1997).
[24] J.P. Perdew and A. Zunger, Phys. Rev. B **23**, 5048 (1981).
[25] N. Troullier and J.L. Martins, Phys. Rev. B **43**, 1993 (1991).
[26] E. Artacho, D. Sánchez-Portal, P. Ordejón, A. García, and J. Soler, Phys. Status Solidi B **215**, 809 (1999).
[27] J. Junquera, O. Paz, D. Sánchez-Portal, and E. Artacho, Phys. Rev. B **64**, 235111 (2001).
[28] H.J. Monkhorst and J.D. Pack, Phys. Rev. B **13**, 5188 (1976).
[29] S. Reich, C. Thomsen, and P. Ordejón, Phys. Rev. B **64**, 195416 (2001).
[30] J.-C. Charlier, P. Lambin, and T.W. Ebbesen, Phys. Rev. B **54**, R8377 (1996).
[31] M. Damnjanović, I. Milošević, T. Vuković, and Sredanović, Phys. Rev. B **60**, 2728 (1999).
[32] X. Blase, private communication.
[33] J.C. Slater, *Quantum Theory of Molecules and Solids* (McGraw-Hill, New York, 1965), Vol. 2.
[34] A. Kleiner and S. Eggert, Phys. Rev. B **64**, 113402 (2001).
[35] The band structure found without a relaxation of the atomic positions is only a rough approximation of the band structure of the rotated tubes, since the atoms are not necessarily in equilibrium. The forces on the atoms and the stress tensor components increased by a factor of 3–6 because of the rotation.
[36] A.M. Rao, J. Chen, E. Richter, U. Schlecht, P.C. Eklund, R.C. Haddon, U.D. Venkateswaran, Y.-K. Kwon, and D. Tománek, Phys. Rev. Lett. **86**, 3895 (2001).
[37] M. Damnjanović, T. Vuković, and I. Milošević, Solid State Commun. **116**, 265 (2000), Table I in the reference contains a small error: For chiral tubes and the $\tilde{k}$ quantum numbers $\tilde{k}_F = 2q\pi/3na$ for $\mathcal{R}=3$ tubes and $\tilde{k}_F=0$ for $\mathcal{R}=1$ nanotubes.
[38] J. Maultzsch, S. Reich, and C. Thomsen, Phys. Rev. B **64**, 121407(R) (2001).
[39] A. Kasuya, Y. Sasaki, Y. Saito, K. Tohji, and Y. Nishina, Phys. Rev. Lett. **78**, 4434 (1997).
[40] P. Kim, T.W. Odom, J.-L. Huang, and C.M. Lieber, Phys. Rev. Lett. **82**, 1225 (1999).
[41] L.C. Venema, J.W. Janssen, M.R. Buitelaar, J.W.G. Wildöer, S.G. Lemay, L.P. Kouwenhoven, and C. Dekker, Phys. Rev. B **62**, 5238 (2000).
[42] Z.M. Li *et al.*, Phys. Rev. Lett. **87**, 127401 (2001).
[43] Z. Yu and L.E. Brus, J. Phys. Chem. B **105**, 6831 (2001).